

THE GALAXY VIEWED WITH H.E.S.S.

Werner Hofmann
for the H.E.S.S. collaboration

Max-Planck-Institut für Kernphysik, 69029 Heidelberg, Germany

ABSTRACT

The H.E.S.S. system of imaging atmospheric Cherenkov telescopes in Namibia has been in full operation since December 2003 and has provided a wealth of exciting new results from the survey of the Galactic plane at VHE energies, and on VHE gamma-ray emission from supernova remnants, binary systems and pulsar wind nebulae.

1. THE H.E.S.S. TELESCOPE SYSTEM

H.E.S.S. is a system of four large (13 m diameter) imaging atmospheric Cherenkov telescopes (Fig. 1), operated by an international collaboration of about 100 physicists. The telescopes [1] are located in the Khomas highland of Namibia, near the tropic of Capricorn. With their cameras [2] containing 960 photomultiplier pixels and covering a 5° field of view, they provide multiple images of gamma-ray (and cosmic-ray) induced air showers in the Cherenkov light emitted by the shower particles, and enable the stereoscopic reconstruction of the shower geometry and, from the observed intensity and the reconstructed distance between telescopes and shower axis, the determination of the shower energy. The full four-telescope system is in operation since December 2003, and was officially inaugurated by the Namibian Prime Minister in September 2004. The telescopes operate about 1000 h per year during moonless night time, recording shower events at a rate of about 300 Hz. Near zenith, the energy threshold - defined as the energy of peak detection rate for typical source spectra - is about 100 GeV, increasing with zenith angle to 250 GeV at 45° and 700 GeV at 60° . The system provides an angular resolution of 0.1° for individual gamma-rays; gamma-ray sources can typically be located with a precision of $1'$ or better, limited for intense sources by systematic errors at the $20''$ level. The sensitivity of the H.E.S.S. telescope system is about one order of magnitude better than previous instruments, and allows to detect sources with a flux of 1% of the Crab Nebula in 25 h of observations.

Highlights from H.E.S.S. include the Galactic plane survey, which unveiled a large number of new VHE gamma-ray sources, the detailed studies of supernova remnants and pulsar wind nebulae, the discovery of gamma rays

from binary systems and the study of emission from the Galactic center region. While the location of H.E.S.S. in the southern hemisphere emphasizes Galactic sources, exciting results have also been obtained for extragalactic objects.

This paper represents an update of a highlight contribution to the 2005 ICRC [3]. Lack of space prevents coverage of all results and the in-depth discussion of the numerous sources; for details and further references, the reader should consult the H.E.S.S. publications cited. Unpublished results should be considered preliminary.

2. THE H.E.S.S. GALACTIC PLANE SURVEY

The H.E.S.S. Galactic plane survey (Fig. 2) was conducted in the summer of 2004 and covered the region of $\pm 30^\circ$ in Galactic longitude and $\pm 3^\circ$ in latitude, at a typical sensitivity of a few % of the Crab flux. In total, 15 new VHE gamma ray sources were discovered during the survey, in addition to three previously known sources in the survey region - the Galactic center, G0.9+0.1, and RX J1713.7-3946. The eight strongest sources, with a post-trial significance exceeding 6σ , were published in [4]; a detailed account of 14 sources, including 6 fainter ones, is given in [5]. In addition, the discovery of a source coincident with the microquasar LS 5039 was presented separately in [6]. The sources line up along the Galactic equator, with a rms spread in latitude of 0.3° , consistent with the scale height of the distribution of molecular gas and with the width of the distribution of supernova remnants and pulsars. Their Galactic origin is confirmed by the fact that nearly all sources are extended, with rms sizes up to 0.2° . H.E.S.S. can typically resolve a source as extended when its rms size exceeds $2'-3'$. For all new sources, energy spectra could be determined [5]; photon indices range from 1.8 to 2.7, with a mean of 2.3, roughly consistent with the expectation for shock wave acceleration of charged particles.

Counterparts for the new sources were searched, primarily in radio- and X-ray catalogs. Five sources could be related to supernova remnants; one example is HESS J1834-087, which nicely coincides with the shell SNR G23.3-0.3 (Fig. 3(a)). A significant fraction of the new sources might be associated with pulsar wind nebulae,



Figure 1. The H.E.S.S. telescope system

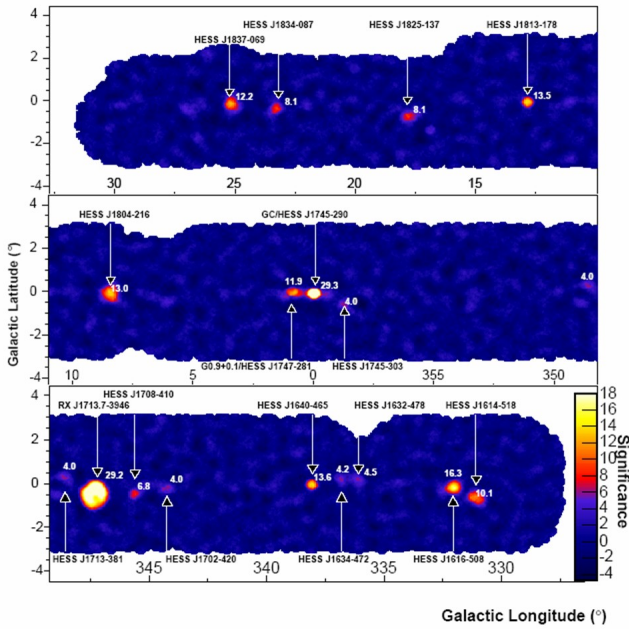


Figure 2. Significance map for the H.E.S.S. survey of the central section of the Galactic plane [5]. Gamma-ray sources are indicated with their HESS J name and (post-trials) significance. The typical energy threshold for this map is 250 GeV. The on-source counts for each coordinate point are integrated over a radius of 0.22° , optimized for slightly extended sources.

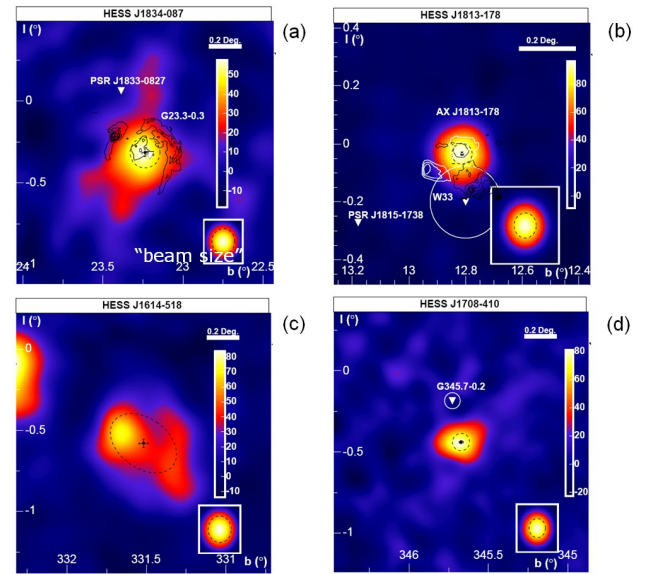


Figure 3. Smoothed gamma-ray excess maps of some of the new Galactic sources, together with potential counterparts in other wavelength ranges. The small inset shows the point spread function after smoothing. (a) HESS J1834-087, coincident with SNR G23.3-0.3 (W41); black contours show the radio emission [41]. (b) HESS J1813-178, with radio contours (black) and ASCA X-ray contours (white). (c) HESS J1614-518 and (d) HESS J1708-410; for both sources no counterpart is known.

3. SUPERNOVA REMNANTS STUDIED WITH H.E.S.S.

although the VHE emission is often offset from the pulsar location – this will be discussed later in more detail. Some of the new sources coincide with EGRET or ASCA unidentified sources. At least three have no counterpart known to us and are sometimes termed “Dark accelerators”.

A H.E.S.S. highlight is the detection of the resolved supernova remnant (SNR) shell of RX J1713.7-3946 (Fig. 4) [7, 8], an object initially discovered in VHE gamma-rays by CANGAROO [9]. TeV gamma ray emission can be clearly traced to the supernova shell, demonstrating that the shock wave accelerates particles to multi-TeV energies, generating photons via interactions with

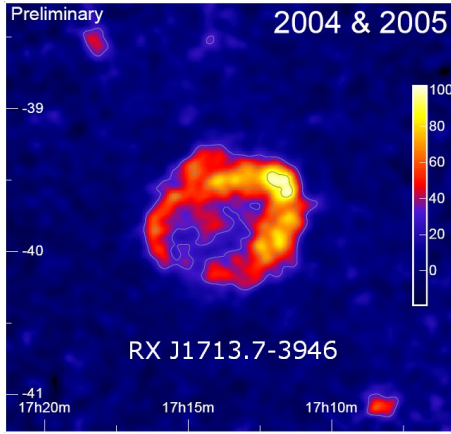


Figure 4. Supernova remnant RX J1713.7-3946 seen in gamma rays

gas – in case of protons - or by Inverse Compton (IC) scattering – in case of accelerated electrons. The energy spectrum of RX 1713.7-3964 has been measured over two decades in energy (Fig. 5), to beyond 30 TeV, and approximately follows a power law with index 2.1 to 2.3,

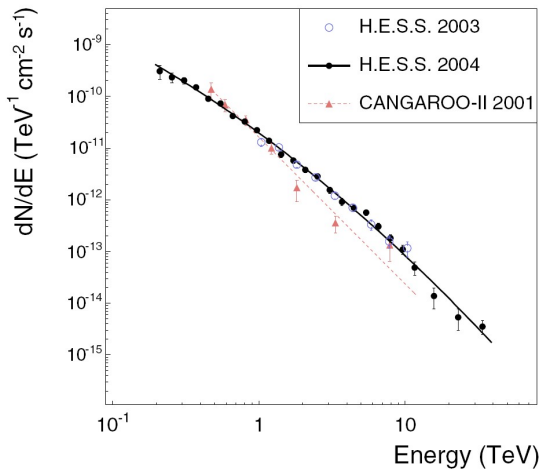


Figure 5. Energy spectrum of gamma rays from RX J1713.7-3964, based on the 2003 and 2004 H.E.S.S. data [8]; also shown are the original CANGAROO points.

with a cutoff or break at the highest energies. The spectral index coincides with predictions of shock-wave acceleration models; the high photon energies which are detected demonstrate that energies of primary particles reach up to 10^{14} eV and beyond. The spectral index is - within errors - constant across the entire remnant.

To probe the emission mechanisms, it is instructive to look at intensities along two orthogonal slices across RX J1713.7-3946 (Fig. 6). One slice goes from the high-intensity region to the low-intensity region (top row of

images), the other (bottom row) in the orthogonal direction. The top gamma-ray slice (left) shows variations in intensity by a factor 3-4; the distribution of gamma rays matches closely the distribution of X-rays (center) [10]. This correlation would be natural if a common population of primary electrons were responsible for X-rays (by synchrotron radiation) and for VHE gamma rays (by IC scattering). For a proton accelerator, one would expect the gamma-ray intensity to correlate with gas density as measured by the CO emission [12] (right); while a certain correlation is visible, it is not nearly as striking as in the case of X-rays. However, comparison with the CO emission as a measure of gas density suffers from the limited depth information. Despite a rough velocity selection corresponding to the suggested 1 kpc distance of the SNR, the molecular clouds, or parts thereof could be located before or behind the remnant. The orthogonal slice (bottom row) illustrates nicely the shell structure; for the correlation with X-rays (middle) and CO intensity (right), the same conclusions as for the first slice apply. However, simple electronic models fail to consistently fit the multiwavelength data (Fig. 7). From the relative levels of

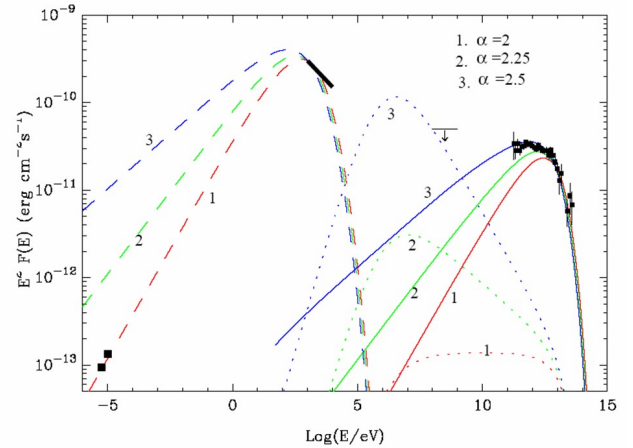


Figure 7. Wideband spectra of synchrotron radiation (dashed), bremsstrahlung (dotted, for a density of $1/\text{cm}^3$) and Inverse Compton radiation (full lines), for a magnetic field around $10 \mu\text{G}$ and an electron injection index of 2.0, 2.25 and 2.5. Also shown are the TeV (H.E.S.S.), X-ray (ASCA) [10] and radio data [11].

X-ray and gamma-ray intensities, a local magnetic field $B \approx 10 \mu\text{G}$ can be determined, assuming that X-rays represent synchrotron radiation ($\sim B^2$) and that the gamma rays are generated in Inverse Compton scattering. A standard E^{-2} electron injection spectrum describes the radio and X-ray spectra, but fails to account for the flat top of the gamma-ray spectrum; the Inverse Compton peak should be visible in the energy range covered by H.E.S.S. With a steeper spectrum, $E^{-2.5}$, the gamma-ray spectrum can be accommodated, but then model predictions overshoot the radio flux [11] by almost two orders of magnitude¹. In contrast, models which use a higher magnetic

¹However, a recent paper [13] points out that improved fits of elec-

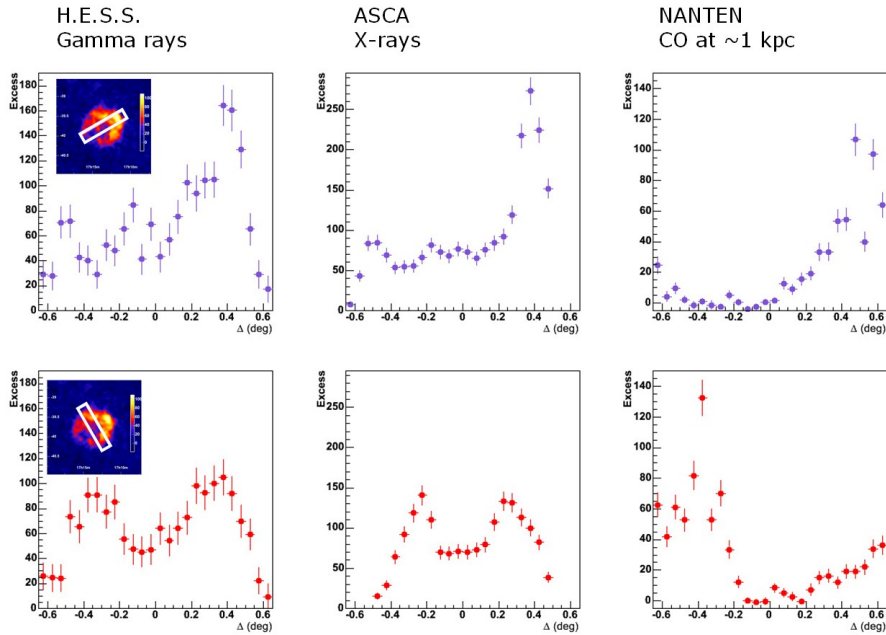


Figure 6. Slices across the remnant RX J1713.7-3946, in the direction from low to high gamma-ray intensity (top row) and in the orthogonal direction (bottom row). Left: rate of gamma rays; middle: rate of X-rays (ASCA [10]); right: CO intensity, measuring the density of interstellar clouds, in the velocity range corresponding to a distance around 1 kpc [12].

field (which suppresses the Inverse Compton component for a given X-ray intensity) and which add gamma-rays generated in proton interactions, achieve a good description of wide-band spectra [14]. In summary, remarkable progress has been made in pinning down SNRs as cosmic accelerators, and there is a preference for a hadronic origin of the high-energy gamma rays; however, fully conclusive evidence is still lacking.

RX J1713-3946 is not the only supernova shell resolved in VHE gamma rays; another nice example is RX J0852.0-4622 (“Vela Junior”), first seen as a gamma-ray source by CANGAROO [15] and now resolved by H.E.S.S. [16] (Fig. 8). Again, gamma-rays and X-rays intensities are highly correlated.

4. H.E.S.S. OBSERVATIONS OF PULSAR WIND NEBULAE

Another interesting class of new TeV gamma-ray sources are pulsar wind nebulae (PWN), which are potentially responsible for a significant fraction of the new sources. A supernova explosion frequently leaves a pulsar behind, which, with its high magnetic and electric fields, generates a steady stream of high-energy electrons and positrons. This pulsar wind blows a hole into the remnant, compressing ejecta in a pulsar wind termination shock, in which the electrons can be re-accelerated. The

tron models can be achieved if higher interstellar radiation fields in the inner Galaxy are taken into account.

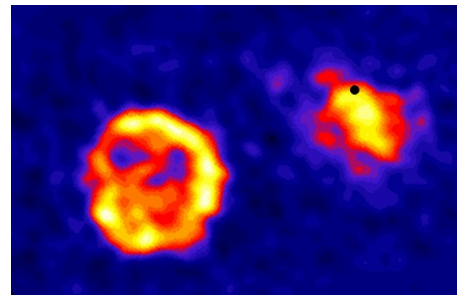


Figure 8. Supernova remnant RX J0852.0-4622 seen in gamma rays. Also visible is the pulsar wind nebula associated with the Vela pulsar; the pulsar location is shown as a black point.

energy content of the pulsar wind is typically a few orders of magnitude lower than the kinetic energy available for particle acceleration in the supernova ejecta, which makes it surprising that pulsar wind nebulae - with the Crab Nebula as the best-studied example - are such prominent sources. The reason is that energy in pulsar wind electrons is far more efficiently converted to gamma rays than the energy of protons and nuclei accelerated in the main supernova shock. Typical radiative life times for electrons are $O(10^3-10^4)$ y, compared to $O(10^7)$ y for protons, which compensates for the deficit in energy. PWN detected in X-rays sometimes appear shifted relative to the pulsar [17, 18]; explanations include a (single-sided) jet-like emission or the “crushing” of one side of the PWN by the reverse shock [19], which is released

when the supernova shock wave has swept up a significant amount of material, generating a back-reaction. If a supernova explodes into an inhomogeneous environment - as most supernovae do - the reverse shock from the side of the denser medium will reach and crush the corresponding side of the PWN while - if observed at the right time - the other half of the PWN is still unaffected.

VHE gamma rays provide an important diagnostic for PWN, since they allow to measure directly the spatial and spectral distribution of high-energy electrons; unlike for X-rays, where emission is governed by the a priori unknown magnetic fields, TeV gamma-ray production is usually dominated by Inverse Compton scattering off the well-known cosmic microwave background. H.E.S.S. has detected a number of extended PWN, among them is Vela X, associated with the Vela pulsar (Fig. 8) [20]. The gamma ray source extends almost a degree south of the pulsar, and features a very hard energy spectrum reaching up to 50 TeV (Fig. 9). The spectrum is clearly curved; a better fit than with a simple power law is obtained with a power law with high-energy cutoff, and a low-energy index around 1.5, which makes this one of the flattest gamma-ray spectra measured, and the first with a peak of the SED in the TeV range. At the location of the Vela pulsar itself, no significant steady or pulsed emission is detected.

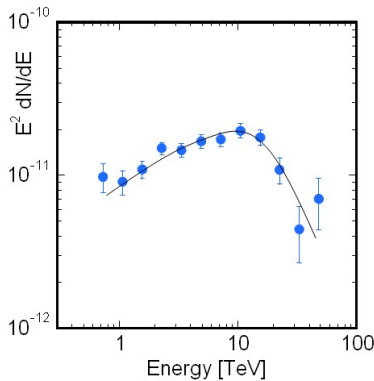


Figure 9. Spectrum of gamma rays from Vela X. The line shows a model calculation assuming an electron population with spectral index of 2 and a cutoff energy of 70 TeV.

Beyond Vela-X, H.E.S.S. has detected a number of sources very likely representing PWN; surprisingly, almost all are displaced with respect to their pulsars. Another interesting PWN is MSH 15-52, associated with the pulsar PSR B1509-58 inside the G 320.4-1.0 / RCW 89 shell (Fig. 10(top)). The elongated and single-sided nebula was seen in ROSAT images [21]; high-resolution Chandra images [22] revealed a jet-like feature. MSH 15-52 was first detected as a gamma-ray source by CANGAROO [23]. H.E.S.S. observations resolve an extended source [24] aligned in the same direction as the Chandra jet feature, and with a power-law energy spectrum extending to well beyond 10 TeV. More recently,

studies of the “Kookaburra” region [25] revealed two new TeV gamma-ray sources [26] (Fig. 10(bottom)), one most likely associated with the pulsar PSR J1420-6048, the other with the “Rabbit” feature presumably resulting from another pulsar. Both sources have relatively hard spectra with spectral index around 2.2, both are extended on the scale of about 10 pc and both are displaced by a similar amount from their pulsars.

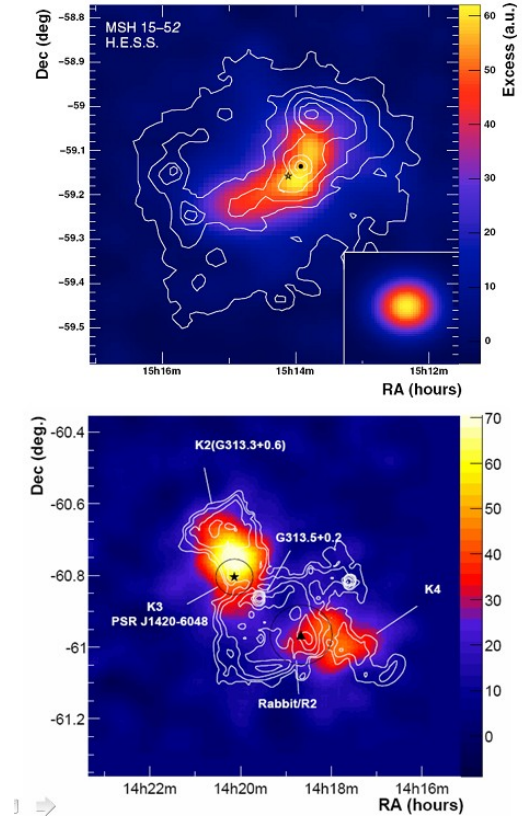


Figure 10. Top: Smoothed gamma-ray excess map from MSH 15-52 [24]. The white contour lines denote the X-ray count rate measured by ROSAT [21]. The black point and the star lie at the pulsar position and at the excess centroid, respectively. The inset shows the point spread function after smoothing. Bottom: Kookaburra region with two gamma-ray sources [26]. White contours are from ATCA 20 cm high resolution images. The black star and triangle mark the positions of the pulsar PSR J1420-6048 and the Rabbit (G313.3+0.1) R2 source. Black circles around these two positions show the approximate extension of the X-ray diffuse emission [25].

A particularly nice candidate for a displaced PWN is HESS J1825-137 [27]. Located south of the pulsar PSR B1823-13, the VHE gamma-ray emission peaks near the pulsar and then falls off towards the south (Fig. 11(left)). Exactly the same feature is seen in X-rays [18], except that the characteristic extension of the nebula is a few arc-minutes rather than a fraction of a degree. A natural explanation is [27] that in the estimated 10 μ G field in the

nebula, the X-ray generating electrons have higher energies than those responsible via Inverse Compton scattering for the VHE gamma rays. The higher-energy X-ray electrons cool faster and have a shorter range. For this source, one for the first time finds a variation of gamma-ray spectra across the source [28]: high-energy gamma-rays emerge from the region close to the pulsar, whereas lower-energy gamma-rays are spread out over a larger region (Fig. 11(right)). These results demonstrate conclusively that the displaced gamma-ray nebula is indeed created by the pulsar.

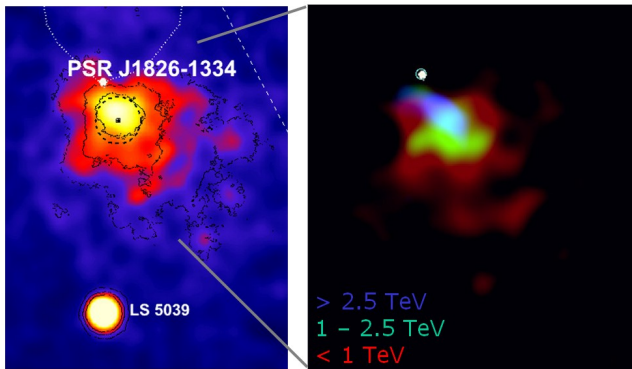


Figure 11. Left: the extended gamma-ray source HESS J1825-137; south of HESS J1825-137 a second (point) source associated with LS 5039 is visible. The white point marks the location of the pulsar. Right: Zoomed-in sky map for different ranges of gamma-ray energy: above 2.5 TeV (blue), 1 to 2.5 TeV (green) and below 1 TeV (red).

One wonders if all pulsars have associated VHE gamma-ray nebulae. A systematic search for gamma-ray counterparts of known pulsars in the region of the Galactic plane survey has resulted in two new PWN candidates, HESS J1809-193 and HESS J1718-385. In fact, among pulsars in the survey region with a spin-down energy flux above 10^{35} ergs/s/kpc², a large fraction is visible as gamma-ray emitters, converting about 1% of their spin-down energy into 1-10 TeV gamma rays. Extrapolated to the full spectrum, this conversion efficiency implies that some 10% of pulsar spin-down energy is fed into high-energy electrons.

5. BINARY SYSTEMS STUDIED WITH H.E.S.S.

A source discovered in the Galactic plane survey in the field of view of HESS J1825-137, HESS J1826-148 (Fig. 11(left)) [6], is coincident with a close binary, LS 5039, consisting of a few-solar-mass compact object - a neutron star or black hole - in a 4 day orbit around a massive star, with a closest approach around 2 stellar radii. The compact object accretes mass from the massive star; the system is particularly remarkable in that VLA radio observations [29] have revealed the existence of two jets, making

this a “microquasar” in close analogy to active galaxies, except that mass and time scales are reduced². Additional recent H.E.S.S. data provide much enhanced significance for this source and allow to probe orbital variation of the gamma-ray emission [31]. Fig. 12(top) shows a periodogram of the gamma-ray flux from LS 5039. A highly significant peak is observed at a period of 3.908 ± 2 days, to be compared with the known orbital period of 3.9060 days. As a cross-check, the nearby source HESS J1837-125 shows no indication of periodicity, eliminating the possibility of instrumental artifacts (lower panel in Fig. 12(top)). The gamma-ray flux folded with the period is shown in Fig. 12(middle) and exhibits a sinusoidal modulation, with a maximum at the inferior conjunction, where the compact object and star line up along the line of sight. At first, it is surprising that maximum emission does not occur at periastron, where the two objects are closest and where both accretion rates and Inverse Compton scattering rates should be maximal. A likely explanation is that the radiation field of the massive star is so strong that gamma-photon absorption by pair production plays an important role provided that the emission region is within about one astronomical unit from the star [32, 33, 34]. At the inferior conjunction, the angle between gamma-rays emitted towards Earth and stellar photons moving roughly in the same direction is minimized, and most gamma-rays are below pair production threshold and escape. Not only the gamma-ray flux but also the energy spectrum varies strongly along the orbit (Fig. 12(bottom)): near maximum flux the spectrum is much harder, with a high-energy cutoff, compared to a steeper power-law spectrum measured around superior conjunction. The spectral variation is hard to explain by photon absorption alone (which predicts significant modulation also at 200 GeV, where the flux shows very little variation), and seems to require an orbital variation both in the emission and absorption patterns. LS 5039 is the first example where periodic VHE gamma ray emission is observed, as is orbital variability of gamma-ray spectra.

A second binary system as a VHE-gamma rays source was discovered in the early phase of H.E.S.S.: PSR B1259-63 is a distant binary, consisting of a pulsar in a highly eccentric 3.4 y orbit around a massive star with a disk-like equatorial wind. The closest approach - last in March 2004 - is about 20 stellar radii. Near periastron, particles potentially accelerated by the pulsar find enhanced targets for generating gamma-rays, both in the form of the intense photon field of the star, and in the form of the wind. In February 2004, H.E.S.S. detected this system as a TeV source [35] (Fig. 13). Surprisingly, however, the light curve - interrupted by full-moon periods - indicates a double-humped shape with a minimum near periastron. This time variation suggests that interactions of the pulsar wind with the disk material dominate the shape of the light curve; alternatively, the strong Inverse Compton cooling at periastron might prevent effi-

²An alternative explanation has been suggested after the conference [30]: LS 5039 could also be represent a pulsar in orbit around the massive star; the ‘jet’ in this case is a cometary pulsar wind tail, shaped by the stellar wind. A clear signature would be a variation of jet angle along the orbit.

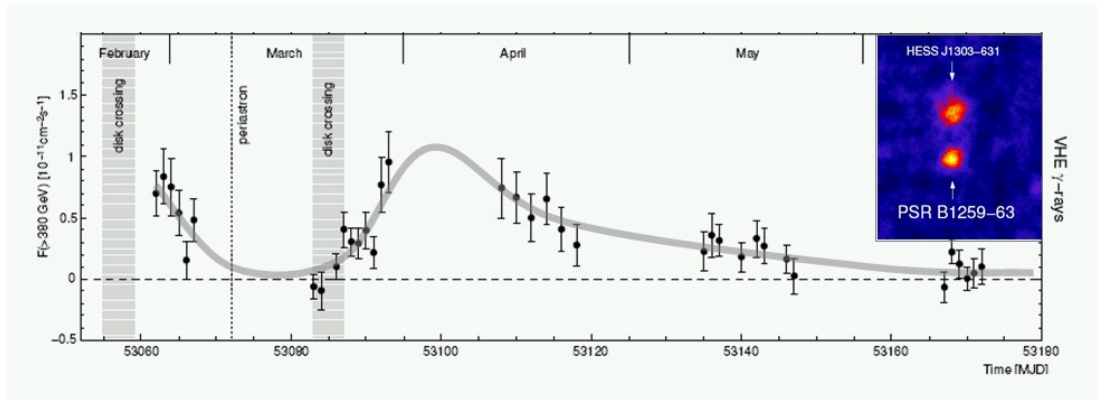


Figure 13. Light curve of VHE gamma rays from the direction of the pulsar PSR B1259-63. The dotted line indicates the point of closest approach between the pulsar and the Be star; the shaded areas show the (approximate) crossing of the disk-like stellar wind. The small inset shows the field around PSR B1269-63 as seen in February 2004, with the second source HESS J1303-631 north of the pulsar.

cient acceleration of electrons.

6. “DARK” SOURCES OF VHE GAMMA-RAYS

Another surprise was the discovery of a second, steady and extended (0.16°) gamma-ray source about 0.5° north of the pulsar, HESS J1303-631 [36] (Inset in Fig. 13). HESS J1303-631 – with a spectrum with photon index $\Gamma \approx 2.4$, reaching up to 10 TeV – is a “dark accelerator” without known counterpart at other wavelengths, despite of follow-up observations with Chandra [37], similar to the first such object TeV J2032+4130 discovered by HEGRA [38]. Dark accelerators are prime candidates for nucleonic accelerators, in which the electron component is either very faint or, more likely, has died out due to radiation cooling [39, 40]. The same interactions which produce gamma-rays by neutral pion decay will of course also represent – by charged pion decay – a steady source of electrons but at least for μG fields the diffuse X-ray emission by these electrons is typically still below the detection threshold.

In the H.E.S.S. Galactic plane survey, several other “dark” TeV sources were discovered. One of the sources which remained unidentified in the original survey paper [4] – HESS J1813-178 – has meanwhile been identified; it coincides with a supernova ring discovered in radio data [42, 41], and also with previously unpublished ASCA [43] and INTEGRAL [43] sources (Fig. 3(b)). Other sources such as HESS J1614-518 and HESS J1708-410 remain unidentified (Fig. 3(c,d)) and more sources of this type have been uncovered in extensions of the original survey. An interesting but open issue is if such “dark” accelerators could make a significant contribution to the density of Galactic cosmic rays.

7. H.E.S.S. OBSERVATIONS OF THE GALACTIC CENTER REGION

A very interesting region is obviously the Galactic center. H.E.S.S. detected two sources near the Galactic center, HESS J1747-281 [44], coincident with the SNR G0.9+0.1 and HESS J1745-290 [45], coincident with the Sgr A complex (Fig. 14(a)). The source of gamma rays in SNR G0.9+0.1 is presumably again a PWN; the gamma ray source is definitely smaller than the SNR shell visible in radio [44]. The origin of the source at the Galactic center – prior to H.E.S.S. seen by CANGAROO [46] and VERITAS [47] with lower significance – is less clear; it could be associated with processes near the central black hole, with the SNR Sgra A East, with the newly discovered PWN G359.95-0.04 [48, 49] located a few arcsec from Sgr A*, or with the annihilation of speculative dark-matter particles (“neutralinos”) left over from the big bang and responsible for structure formation in the universe; the density of such particles should peak as $r^{-\alpha}$ at the Galactic center, with $\alpha \geq 1$ derived from many-body simulations. The location of the H.E.S.S. source is within the $20''$ systematic pointing errors fully consistent with Sgr A*, but an origin in Sgr A East cannot safely be excluded. A possible clue could therefore come from the exact angular distribution of the gamma rays (Fig. 15(a)). Indeed, while the peak at small angular distance from Sgr A* is essentially consistent with the angular resolution of the instrument, the angular distribution has a pronounced tail, which is not accounted for by the point spread function. A fit based on dark-matter distributions yields good agreement for $\alpha \approx 1.0$. More constraints concerning the nature of the source can come from the spectrum and the time variability of the flux. The measured spectrum Fig. 15(b) is a pure power law, extending, with the most recent H.E.S.S. data, over two decades in energy. The measured flux is consistent with constant emission, on scales of (2) years, months, days and hours. However, caveats to be listed are that the to-

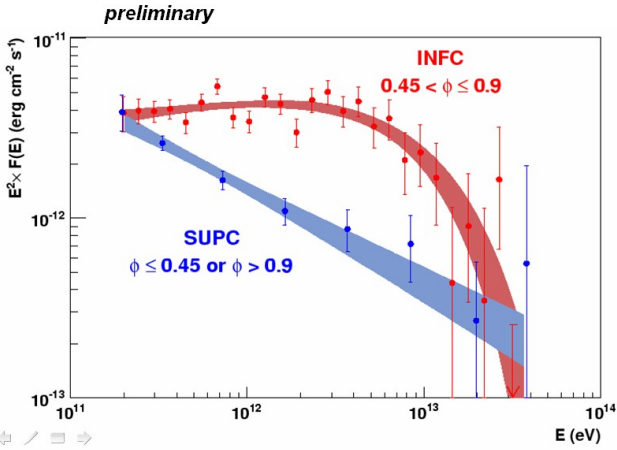
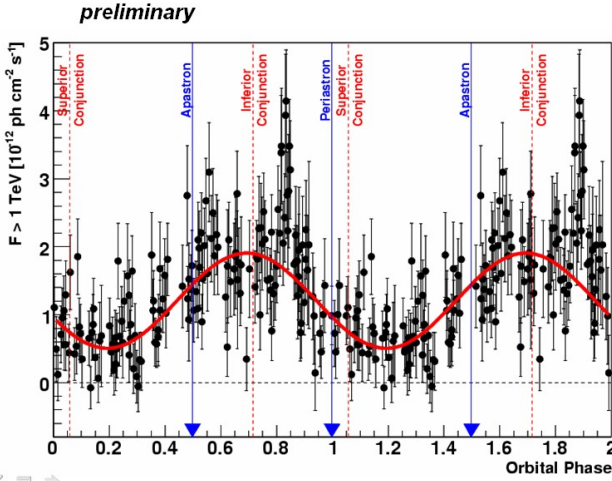
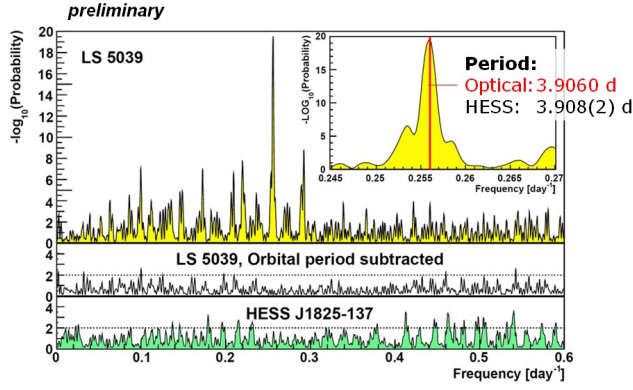


Figure 12. Top: periodogram of the gamma-ray emission from LS 5039. The smaller peaks result from beats between the orbital period and observation gaps and disappear once the dominant period is subtracted (middle panel). The source HESS J1837-125 in the same field of view shows no modulation (bottom panel). Middle: period-folded gamma ray flux showing a maximum near inferior conjunction. Bottom: gamma-ray spectra in the high-flux region around superior conjunction and in the low-flux region around inferior conjunction [31].

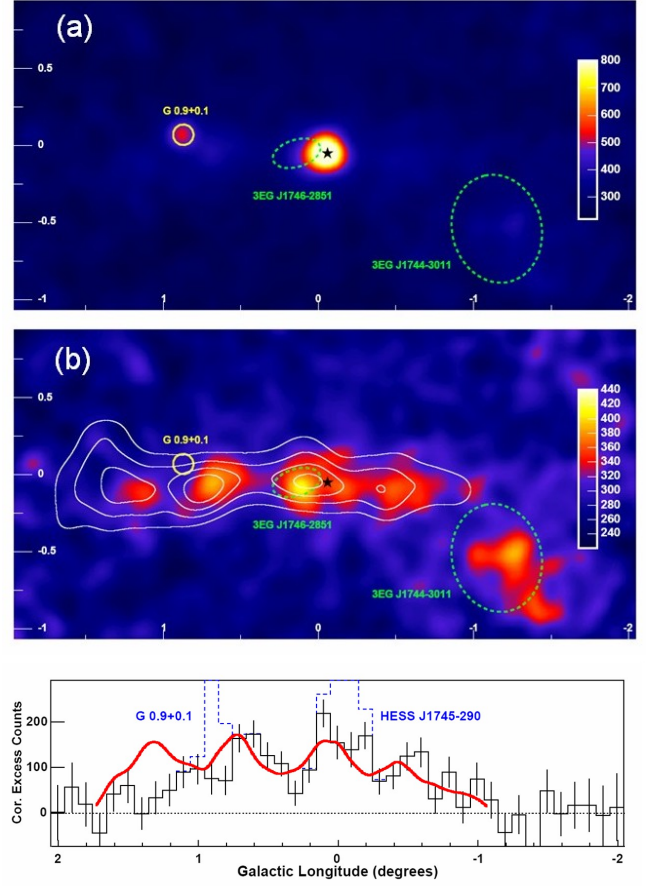


Figure 14. (a) Gamma-ray sky map of the Galactic center region, showing the supernova remnant G0.9+0.1 and Sgr A as prominent sources. (b) Sky map after subtraction of point sources at the locations of G0.9+0.1 and Sgr A, revealing a band of diffuse gamma-ray emission. White contours indicate the density of molecular gas, traced by its CS emission [53]. (c) Slice along Galactic longitude, showing the diffuse gamma-ray excess after subtraction of the point sources (which are shown as dashed lines). The red curve shows the density of molecular gas, traced by the CS emission.

tal integrated observation time in 2003/4 was about 40 h, so flares might have been missed. Also, short flares (on daily or hourly time scales) must have a significant amplitude (flux variations of factors of a few) to be detectable. Nevertheless, the steady emission disfavors processes in the immediate vicinity of the black hole Sgr A*. Concerning the dark-matter signature, the observed power law spectrum does not match the typical (quark or gluon-fragmentation type) gamma-ray spectra from neutralino annihilation [50] (Fig. 15(b)), even ignoring the fact that most models prefer neutralinos in the energy range up to 1 TeV, not capable of generating spectra which extend beyond 10 TeV. Classical SUSY neutralinos have strongly curved spectra, at variance with observations. Models based on Kaluza-Klein dark matter particles pro-

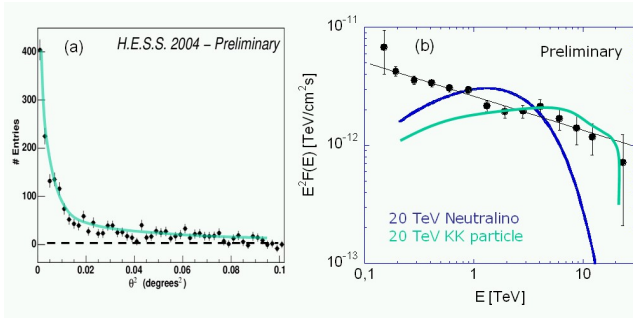


Figure 15. (a) Angular distribution of the gamma-ray emission from the Sgr A source HESS J1745-290. Shown is the distribution in the angle θ^2 relative to the source. (b) Spectral energy density of HESS J1745-290. Lines: spectra resulting from the annihilation of typical MSSM neutralinos and from Kaluza-Klein dark-matter particles [51]. (Preliminary)

vide enhanced few-body decay modes and flatter spectra [51], and are capable of reproducing the early H.E.S.S. 2003 data set. The full 2004 spectrum, extending down to 150 GeV, is not reproduced by these models (Fig. 15(b)). Hence, it seems very improbable that the full gamma ray signal from the Galactic center is caused by dark matter annihilation. A partial contribution, in particular at low energies, cannot be excluded.

The extended component of gamma-ray emission in the Sgr A region could also be related to diffuse emission of cosmic rays interacting with the dense molecular clouds in this region; the resulting gamma rays flux should be detectable with H.E.S.S. Indeed, subtracting the two point sources HESS J1745-290 and HESS J1747-281 leaves a clear excess extending along the Galactic ridge, between -1° and 1° longitude, and a (rms) width of about 0.2° in latitude (Fig. 14(b)) [52]. Apart from a region at $l \approx 1.5^\circ$, the excess traces the density of molecular clouds estimated via their CS emission [53] (Fig. 14(c)). The spectrum of the diffuse component is similar to the spectrum observed for the central source HESS J1745-290, and has a spectral index of 2.3, harder than expected for gamma rays from interactions of cosmic rays with the spectrum locally measured on Earth, and showing an excess over the such predicted spectrum at higher energies. Given the proximity of accelerators and targets in the complex region near the Galactic center, a harder spectrum is expected since effects of diffusion and escape should be reduced. An open question remains the deficit of emission - compared to the density of molecular clouds - around $l \approx 1.5^\circ$. One speculative explanation is that the cosmic rays interacting with the clouds were “recently” (some 10000 years ago) generated by an accelerator near $l = 0$ and did not yet have sufficient time to diffuse beyond $|l| = 1^\circ$. An alternative explanation for the diffuse gamma-ray band is provided by assuming a superposition of O(10) point-like sources, with a distribution governed by that of the molecular gas.

In summary, the first results from H.E.S.S. have revealed a number of interesting new objects in the TeV sky – among them many extended sources – providing a new handle to study processes in the sources. The H.E.S.S. results also demonstrate that Cherenkov instruments of the latest generation have passed a critical sensitivity threshold, where real VHE gamma-ray astronomy becomes feasible.

ACKNOWLEDGEMENTS

This report represents the cumulative effort by the H.E.S.S. collaboration in building and operating the instrument and in analyzing the data. The author would like to emphasize in particular the key contributions by many of our outstanding students and postdocs, who deserve the lion’s share of the credit for the success of the H.E.S.S. project.

REFERENCES

1. K. Bernlöhner et al., *Astropart. Phys.* 20 (2003) 111
2. P. Vincent et al., 2003, in *Proc. 28th ICRC, Tsukuba* (Univ. Academy Press, Tokyo), 2887
3. W. Hofmann, *Proc. 29th ICRC, Pune, 2005, Vol. 10*, p. 97
4. F.A. Aharonian et al., *Science* 307 (2005) 1938
5. F.A. Aharonian et al., *ApJ* 636 (2006) 777
6. F.A. Aharonian et al., *Science* 309 (2005) 746
7. F.A. Aharonian et al. (HESS Collaboration), *Nature* 307 (2005) 1938
8. F.A. Aharonian et al. (HESS Collaboration), *A&A* 449 (2006) 223
9. H. Muraishi et al., *A&A* 354 (2000) L57
10. Y. Uchiyama et al., *AIP Conf. Proc.* 745, p. 305 (2005)
11. J.S. Lazendic et al., *ApJ* 602 (2004) 271
12. Y. Fukui et al., *PASJ* 55 (2003) L61
13. T.A. Porter, I.V. Moskalenko, A.W. Strong, *astro-ph/0607344* (2006)
14. E.G. Berezhko, H.J.Völk, *astro-ph/0602177* (2006)
15. H. Katagiri et al., *ApJ* 619 (2005) L163
16. F.A. Aharonian et al. (HESS Collaboration), *A&A* 437 (2005) L7
17. C.B. Markwardt, H.B. Ögelmann, *ApJ* 480 (1997) L13

18. B.M. Gaensler et al., *ApJ* 588 (2003) 441
19. J.M. Blondin, R.A. Chevalier, D.M. Frierson, *ApJ* 563 (2001) 806
20. F.A. Aharonian et al. (HESS Collaboration), *A&A* 448 (2006) L43
21. E. Trussoni et al., *A&A* 306 (1996) 581
22. B.M. Gaensler et al., *ApJ* 569 (2002) 878
23. T. Sako et al., *ApJ* 537 (2000) 422
24. F.A. Aharonian et al., *A&A* 435 (2005) L17
25. C.Y. Ng, M.S.E. Roberts, R.W. Romani, *ApJ* 627 (2005) 904
26. F.A. Aharonian et al. (HESS Collaboration), *A&A* 456 (2006) 245
27. F.A. Aharonian et al. (HESS Collaboration), *A&A* 442 (2005) L25
28. F.A. Aharonian et al. (HESS Collaboration), *astro-ph/0607548* (2006)
29. J.M. Paredes et al., *Science* 288 (2000) 2340
30. G. Dubus, *astro-ph/0605287* (2006)
31. F.A. Aharonian et al. (HESS Collaboration), *astro-ph/0607192* (2006)
32. G. Dubus, *astro-ph/0509633* (2005)
33. W. Bednarek, *MNRAS* 368 (2006) 579
34. M. Boettcher, C. D. Dermer, *ApJ* 634 (2005) L81
35. F.A. Aharonian et al. (HESS Collaboration), *A&A* 442 (2005) 1
36. F.A. Aharonian et al. (HESS Collaboration), *A&A* 439 (2005) 1013
37. R. Mukherjee, J.P. Halpern, *ApJ*. 629 (2005) 1017
38. F.A. Aharonian et al. (HEGRA Collaboration) *A&A* 431 (2005) 197
39. A. Atoyan, J. Buckley, H. Krawczynski, *ApJ* 642 (2006) L153
40. R. Yamazaki et al., *MNRAS* 371 (2006) 1975
41. R.L. White, R.H. Becker, D.J. Helfand, *AJ* 130 (2005) 586; D.J. Helfand, R.H. Becker, R.L. White, *astro-ph/0505392* (2005)
42. C.L. Brogan et al., *ApJ* 629 (2005) L105
43. P. Ubertini et al., *ApJ* 629 (2005) L109
44. F.A. Aharonian et al. (HESS Collaboration), *A&A* 432 (2005) L25
45. F.A. Aharonian et al. (HESS Collaboration), *A&A* 425 (2004) L13
46. K. Tsuchiya et al., *ApJ* 606 (2004) L115
47. K. Kosack et al., *ApJ* 608 (2004) L97
48. Q.D. Wang, F.J. Lu, E.V. Gotthelf, *MNRAS* 367 (2006) 937
49. J.A. Hinton, F.A. Aharonian, *astro-ph/0607557* (2006)
50. P. Gondolo et al., 2004, <http://www.physto.se/~edsjo/darksusy/>
51. L. Bergstrom et al., *Phys. Rev. Lett.* 94 (2005) 131301
52. F.A. Aharonian et al. (HESS Collaboration), *Nature* 439 (2006) 695
53. M. Tsuboi, H. Toshihiro, N. Ukita, *ApJSS* 120 (1999) 1